

Fingerprinting triangular-lattice antiferromagnet by excitation gaps

K. E. Avers^{1,2,3}, P. A. Maksimov,⁴ P. F. S. Rosa,¹ S. M. Thomas¹, J. D. Thompson¹, W. P. Halperin^{1,2},
R. Movshovich¹ and A. L. Chernyshev⁵

¹*Los Alamos National Laboratory, Los Alamos, New Mexico 87545, USA*

²*Department of Physics and Astronomy, Northwestern University, Evanston, Illinois 60208, USA*

³*Center for Applied Physics and Superconducting Technologies, Northwestern University, Evanston, Illinois 60208, USA*

⁴*Bogolyubov Laboratory of Theoretical Physics, Joint Institute for Nuclear Research, Dubna, Moscow Region 141980, Russia*

⁵*Department of Physics and Astronomy, University of California, Irvine, California 92697, USA*



(Received 4 February 2021; accepted 3 May 2021; published 21 May 2021)

CeCd₃As₃ is a rare-earth triangular-lattice antiferromagnet with large interlayer separation. Our field-dependent heat capacity measurements at dilution fridge temperatures allow us to trace the field evolution of the spin-excitation gaps throughout the antiferromagnetic and paramagnetic regions. The distinct gap evolution places strong constraints on the microscopic pseudospin model, which, in return, yields a close *quantitative* description of the gap behavior. This analysis provides crucial insights into the nature of the magnetic state of CeCd₃As₃, with a certainty regarding its stripe order and low-energy model parameters that sets a compelling paradigm for exploring and understanding the rapidly growing family of the rare-earth-based triangular-lattice systems.

DOI: [10.1103/PhysRevB.103.L180406](https://doi.org/10.1103/PhysRevB.103.L180406)

Rare-earth-based quantum magnets are of great current interest, as they naturally combine the effects of strong spin-orbit coupling (SOC), which entangles magnetic degrees of freedom and orbital orientations [1,2], with that of the geometric frustration of the lattices bearing a triangular motif, long anticipated as leading to exotic ground states and excitations [3,4]. A remarkable recent surge in the studies of quantum anisotropic-exchange magnets in general and rare-earth-based triangular-lattice (TL) materials in particular is propelled by an avalanche of the newly synthesized compounds [5–22] and theoretical insights into their models [4,23–28]. Rare-earth materials provide an ideal platform for the search of novel phases as they host short-range and highly anisotropic exchange interactions of their effective spin degrees of freedom due to strong SOC and the highly localized nature of the *f* orbitals.

In this Letter, we present low-temperature heat capacity measurements of a Ce-based representative member of this family of materials, CeCd₃As₃, in a regime that has not been accessed in the earlier studies [29]. These measurements enable us to construct the magnetic field-temperature (*H-T*) phase diagram of CeCd₃As₃ and determine the field evolution of the spin-excitation gaps in its spectrum throughout the transition from a frustrated antiferromagnetic (AF) to a paramagnetic (PM) state. We augment these results with a theoretical analysis that yields close agreement with a distinct field dependence of the gaps and allows us to unequivocally identify the ground state of CeCd₃As₃ as being in a stripe phase. The phenomenological constraints on the key parameters of the microscopic model result in robust certainty regarding the ground state and parameter region of the general phase diagram of the anisotropic-exchange TL systems to

which CeCd₃As₃ likely belongs. Our approach is expected to enable a better understanding of the rapidly growing family of rare-earth-based TL materials.

Material and Methods. CeCd₃As₃ crystallizes as thin ($\sim 1 \times 1 \times 0.2$ mm³), platelike crystals in the hexagonal *P6₃/mmc* space group in which Ce⁺³ ions form two-dimensional (2D) triangular lattices that are widely spaced along the *c* axis, as shown in the Supplemental Material (SM) [30]. Its low-temperature magnetization is a characteristic of an easy-plane anisotropy with a ratio of Landé *g* factors $g_{ab}/g_c \sim 5$ [29–31]. Additional experimental details and crystal-field analysis of magnetic susceptibility/magnetization are provided in the SM [30]. Here we focus on our study of the specific heat and its theoretical modeling.

H-T phase diagram. In zero field, CeCd₃As₃ orders at $T_N = 410(20)$ mK, in agreement with a recent report [29] of AF ordering at $T_N \sim 420$ mK. At T_N , only about one quarter of the entropy of the ground state doublet $R \ln 2$ is recovered [30]. The substantial difference between T_N and the *ab*-plane Curie-Weiss (CW) temperature $\theta_{CW} = -4.5$ K also suggests a large degree of frustration in CeCd₃As₃ [32], although with the caveat that the CW temperature can serve as only a crude estimate of the spins' exchange strength in rare-earth materials.

For magnetic fields applied in the *ab* plane, T_N increases, reaches its maximum of 500(30) mK near 2 T, and is suppressed at higher fields [see Figs. 1 and 2(a)]. Above 3.5 T, at temperatures above the sharp feature that is identified with the magnetic ordering, specific heat also exhibits a shoulderlike anomaly denoted as T_U in Fig. 2(b). In Fig. 1, we highlight the crossover (XO) region between these two features as a shaded

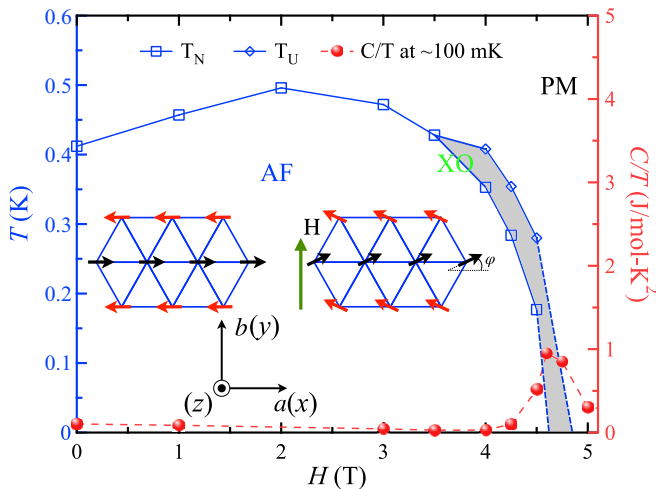


FIG. 1. Open symbols are T_N and T_U vs in-plane field H from the heat capacity data in Figs. 2(a) and 2(b); solid circles are C/T values at 100 mK, and lines are guides to the eye. A crossover (XO) region between T_N and T_U is highlighted. Inset: sketch of the stripe-x AF phase in zero and finite field (see text).

area. Both anomalies are suppressed to zero temperature by a magnetic field near 4.7–4.8 T, suggesting a quantum critical point (QCP) within that field range. As shown in Fig. 1, this region of the phase diagram demonstrates a significant enhancement of the specific heat at a reference low temperature of 100 mK.

Specific heat, T_N , and T_U . Specific heat data for CeCd_3As_3 are presented in Fig. 2 for several field and temperature regimes. The data up to 3 T are shown in Fig. 2(a). They demonstrate the nonmonotonic T_N field dependence, characterized by an initial increase followed by a suppression. Such an increase indicates an enhancement of the AF order with field and is known to occur in several quantum magnets and their models [33–35], wherein this effect is associated with the field-induced suppression of quantum or thermal spin fluctuations or a reduction of frustration. Given our subsequent analysis of the nature of its magnetic ordered state, we ascribe the increase of T_N in the case of CeCd_3As_3 to a field-induced suppression of critical fluctuations related to the phase transition (see the SM [30]).

As shown in Fig. 2(b) for fields 4 T and above, specific heat acquires an additional shoulderlike feature at $T_U > T_N$, giving rise to an XO region between the two temperatures (see also Fig. 1). It appears that the line of T_N transitions continues through 3.5 T with no inflection. Both T_U and T_N decrease towards zero temperature at higher fields, in agreement with the expected suppression of the AF order parameter to zero at a QCP. For the XO region of the phase diagram, we note that while some frustrated TL models consistently have a two-peak structure in their specific heat [36], the second, higher-temperature anomaly at T_U in Fig. 2(b) could also be related to a field-induced high density of states in the magnon spectrum (see Ref. [30]).

Specific heat and low T . Figure 2(c) focuses on the low- T heat capacity. As already indicated in Fig. 1, the behavior of C/T in this temperature range near a presumptive QCP is

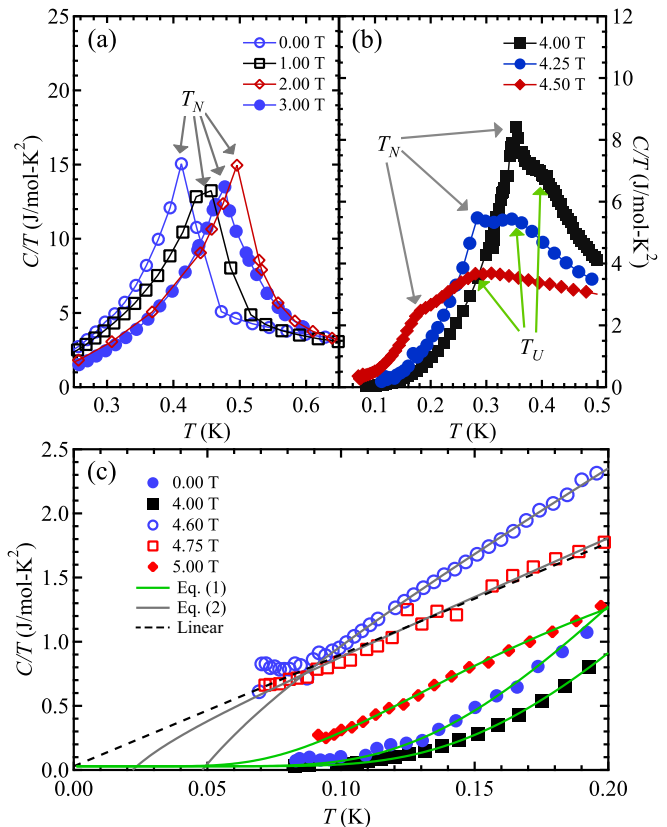


FIG. 2. Specific heat C/T vs T shows (a) the nonmonotonic field dependence of T_N for $H < 3.5$ T, (b) the emergence of T_U and the XO region for $H > 3.5$ T (lines are guides to the eye), (c) the low- T dependence of C/T away from and at the QCP together with the fits from Eqs. (1) and (2) (lines).

drastically different from that in other fields regions. It should also be noted that the QCP region is where universal scalings are expected to dictate the T dependence of all thermodynamic quantities [37].

Figure 2(c) also displays the specific heat as a function of T for several representative fields away from the QCP region (solid symbols). At $T = 100$ mK, C/T is small up to 4.25 T and is suppressed again in fields greater than 5 T. Moreover, the temperature dependence of C/T in Fig. 2(c) in fields outside of the critical region clearly indicates activated behavior characteristic of gapped systems, as we elaborate below.

The enhancement in low- T entropy, manifested as a buildup of area under the C/T vs T curves, occurs for fields between 4.25 and 5 T. This results in the large C/T values at 100 mK shown in Fig. 1. The value of C/T at 100 mK is substantially enhanced, reaching a maximum of about 1 J/mol K² at 4.6 T. It is also accompanied by a distinct change in the temperature dependence, shown in Fig. 2(c) for 4.6 and 4.75 T (open symbols), that is indicative of a power law in T . The rise in C/T below 80 mK for $H = 4.6$ T is likely due to our calorimeter setup not accurately accounting for longer internal thermal relaxation times in this H - T range.

Low- T asymptotes. The leading contribution to the heat capacity from a 2D gapped excitation can be obtained by approximating its energy as $\varepsilon_{\mathbf{k}} \approx \Delta + \mathbf{J}\mathbf{k}^2$ near the minimum

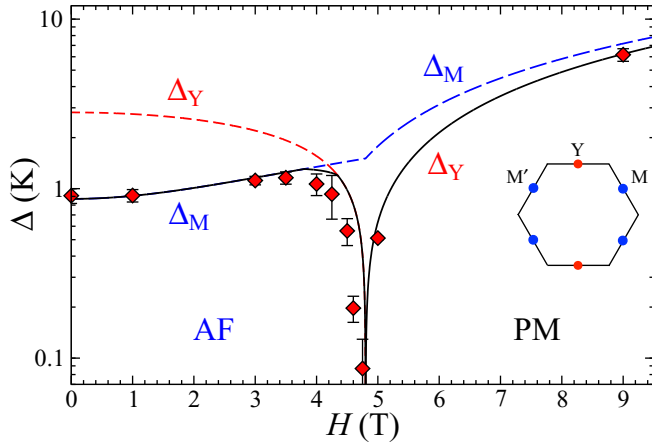


FIG. 3. Δ vs H obtained using Eqs. (1) and (2) (symbols). The excitation spectrum gaps at the ordering vector Y (Δ_Y) and complementary M point (Δ_M) for the parameters of the model (3) discussed in text. Inset: Brillouin zone with the Y and M points for the stripe phase in Fig. 1.

gap Δ and J parametrizing the bandwidth,

$$C(T)/T = A(x^2 + 2x + 2)e^{-x} + b + O(e^{-2x}), \quad (1)$$

where $x = \Delta/T$, $A \sim 1/J$, and a small constant offset b of 0.029 J/mol K² is introduced to account for a calorimeter background heat capacity in all our fits [30]. The 2D activated behavior of Eq. (1) fits very well all C/T data up to 200 mK for fields away from the QCP region, as is demonstrated in Fig. 2(c) (see also Ref. [30]). Since the fit in Eq. (1) is controlled by a single parameter Δ , this analysis allows us to accurately trace the field dependence of the lowest excitation gap in CeCd₃As₃.

For systems with continuous spin symmetries, the field-induced PM to AF transition is of the Bose-Einstein condensation type [37,38]. In our case, because SOC leaves no continuous symmetries intact, this transition is of a different universality class, characterized by the closing of the excitation spectrum gap in a relativistic manner, $\varepsilon_{\mathbf{k}} \approx \sqrt{\Delta^2 + J^2 \mathbf{k}^2}$ [37]. This implies an acoustic mode at the QCP, $\varepsilon_{\mathbf{k}} \propto |\mathbf{k}|$ (dynamical exponent $z=1$), leading to a universal 2D scaling, $C(T) \propto T^2$, at the transition field. The gap closure also explains the peak in C/T vs field in Figs. 1 and 2(c) near the QCP.

At 4.75 T, CeCd₃As₃ appears to be close to the QCP, as is indicated by the linear fit of C/T (dashed line) in Fig. 2(c), which is indicative of gapless excitations. For small gaps, we obtain a modified scaling,

$$C(T)/T \approx AT(1 - x^2/\alpha) + b, \quad (2)$$

with $\alpha = 12\zeta(3)$, valid down to $T \sim \Delta/2$ [30]. Equation (2) provides an excellent fit to the 4.6 and 4.75 T data sets in Fig. 2(c) (solid lines), putting an upper bound on Δ at 4.75 T of $\lesssim 90$ mK and of ≈ 200 mK at 4.6 T.

Gaps and other phenomenologies. The spectrum gap Δ , extracted from the specific heat data using Eqs. (1) and (2), is shown in Fig. 3 vs H . The semilog scale is to accommodate $\Delta \approx 6$ K at 9 T deep in the PM phase. Most of the results in Fig. 3 use $C(T)$ data from the temperature window 0–

200 mK and are checked for stability by varying this fitting range. Error bars combine internal quality of the fits with such variations (see the SM [30]).

The zero-field gap of 0.91(9) K is compatible with the CW temperature [29,30] and shows no sign of closing below the QCP, implying that the AF phase of CeCd₃As₃ evolves continuously with H . Magnetization data corroborate this assertion [30], showing no traces of the plateaulike phase transitions emblematic of TL magnets [39,40].

The field dependence of Δ demonstrates an essential feature. It shows a gradual increase to about 1.1 K at 3.5 T, followed by an abrupt closing upon approaching the critical field. This nonmonotonic behavior is an important distinguishing hallmark that allows us to unambiguously identify the ordered state of CeCd₃As₃.

Model. For Kramers ions in layered compounds, crystal field effects (CEFs) lead to an energy splitting of the local Hilbert space of the rare-earth ion magnetic moment into a series of doublets [41]. At temperatures much lower than the crystal field splitting, the lowest Kramers doublets, naturally parametrized as effective pseudospins $S = \frac{1}{2}$, are responsible for the dominant magnetic properties of insulating materials. Because of the entanglement with the orbital orientations that are tied to the lattice due to CEFs, the pairwise interactions of these pseudospins *a priori* retain no spin-rotational symmetries [4,23]. Instead, it is the discrete symmetries of the lattice that restrict possible forms of the bond-dependent interactions. Together with the localized nature of f orbitals that limits the ranges of interactions, these symmetries lead to generic Hamiltonians that are expected to adequately describe *all* rare-earth-based Kramers compounds on a given lattice [24].

For a layered TL structure, the relevant point-group symmetry operations allow four terms in the Hamiltonian that can be separated into bond-independent, H^{XXZ} , and bond-dependent, H^{bd} , parts (see Ref. [27]),

$$\begin{aligned} \mathcal{H} &= \sum_{(ij)} (H_{(ij)}^{XXZ} + H_{(ij)}^{bd}) + \sum_{(ij)_2} H_{(ij)_2}^{XXZ}, \\ H_{(ij)_m}^{XXZ} &= J_m (S_i^x S_j^x + S_i^y S_j^y + \bar{\Delta} S_i^z S_j^z), \\ H_{(ij)}^{bd} &= 2J_{\pm\pm} [(S_i^x S_j^x - S_i^y S_j^y) \tilde{c}_\alpha - (S_i^x S_j^y + S_i^y S_j^x) \tilde{s}_\alpha] \\ &\quad + J_{z\pm} [(S_i^y S_j^z + S_i^z S_j^y) \tilde{c}_\alpha - (S_i^z S_j^z + S_i^z S_j^z) \tilde{s}_\alpha], \end{aligned} \quad (3)$$

where $\tilde{c}(\tilde{s})_\alpha = \cos(\sin) \tilde{\varphi}_\alpha$, $\tilde{\varphi}_\alpha$ are angles of the primitive vectors with the x axis, $\tilde{\varphi}_\alpha = \{0, 2\pi/3, -2\pi/3\}$, and $\{x, y, z\}$ are the crystallographic axes (see Fig. 1). The bond-independent exchange constants J_m are J_1 and J_2 for the first- and second-neighbor couplings, respectively. Following prior works [26,42], we use a minimal extension of the model by the J_2 term with the same XXZ anisotropy $\bar{\Delta}$. In an external field, Zeeman coupling

$$\mathcal{H}_Z = -\mu_B \sum_i [g_{ab} (H_x S_i^x + H_y S_i^y) + g_c H_z S_i^z] \quad (4)$$

contains anisotropic g factors of the pseudospins that reflect the buildup of the ground-state doublets from the states of the \mathbf{J} multiplet of the rare-earth ions by a combined effect of SOC and CEFs. The in-plane g factor is uniform because of the TL threefold symmetry [43].

Phase identification. As the model (3) has no spin-rotational symmetries [23,26], one expects gapped excitations throughout its phase diagram, but accidental degeneracies render most of the phases, such as well-known 120° phase and the nearby incommensurate phases, nearly gapless [27,44]. Of the remaining phases, the CeCd_3As_3 phenomenology of a single-phase field evolution and a sizable spin-excitation gap strongly suggests so-called stripe phases as prime contenders for its ground state. In a stripe phase, ferromagnetic rows of spins arrange themselves in an AF fashion (see the inset in Fig. 1). In particular, as we argue in this work, the nonmonotonic field dependence of the gap is a hallmark of the stripe phases. An alternative scenario of the strong Ising limit leads to phases and transitions [40,45] that are incompatible with the phenomenology of CeCd_3As_3 (see the SM [30] for more detail).

Most importantly, the field evolutions of the spin-excitation spectrum in the stripe phase, at the QCP, and in the spin-polarized PM phase are all in accord with our results for CeCd_3As_3 . Specifically, the spectrum minima in zero field are *not* associated with the ordering vector (identified as a Y point in Fig. 3) but are complementary to it (M points in the Brillouin zone). This feature is characteristic of systems with significant frustrating bond-dependent interactions [27,28]. In an applied field, it is the gap at the ordering vector that must close, leading to a rather abrupt switch of the minimal gap between the M and Y points, as demonstrated in Fig. 3 for a choice of parameters in model (3) discussed next.

Model parameters. Assuming a stripe ground state, we obtain the field evolution of spin excitations for model (3) in the AF and PM phases. There are two empirical quantities that provide strong constraints on the model parameters: the value of the critical field H_s , which we take as 4.8 T, allowing for an ambiguity in the QCP for CeCd_3As_3 , and the zero-field gap Δ_0 , taken as 0.87 K to account for an uncertainty of the fit. Qualitatively, with $g_{ab} \approx 2$ known from the in-plane magnetization data [30,31], the empirical value of H_s strongly binds the cumulative exchange term, $J_1 + J_2$, while Δ_0 restricts the $J_{\pm\pm}$ anisotropic-exchange term (see the SM [30] for details).

We find that the second anisotropic-exchange term, $J_{z\pm}$, has a minor effect on the spectrum [27] and neglect it in our consideration. This mild simplifying assumption leaves two types of stripe states, stripe- x and stripe- y , which correspond to spins along and perpendicular to the bonds of the lattice, respectively, indistinguishable up to a change in the sign of the $J_{\pm\pm}$ term and a switch of the field direction from $H \parallel b$ to $H \parallel a$. Because experiments in CeCd_3As_3 have not discriminated between the in-plane field directions, we take a minimal-model approach [30] by assuming $J_{\pm\pm} < 0$, which corresponds to stripe- x with H along the b direction, as shown in Fig. 1.

We have found that the excitation gaps are virtually insensitive to the value of the XXZ anisotropy $\bar{\Delta}$, which is loosely bound in the range of 0.5–1.5 by the out-of-plane saturation field, extrapolated from $M(H)$ data [30]. The situation is similar to the ratio J_2/J_1 , which does not affect observables at the fixed total $J_1 + J_2$. Thus, by taking XXZ anisotropy $\bar{\Delta} = 1$ and making an *ad hoc* choice of $J_2/J_1 = 0.1$ for the

highly localized f orbitals, for the empirical H_s and Δ_0 we obtain $J_1 \approx 1.19$ K and $J_{\pm\pm} \approx -0.31$ K [30]. With these model parameters, we derive the field evolution of the gaps shown in Fig. 3.

Our results show a gradual increase of the magnon gap energy Δ_M vs field at the complementary M point and concurrent decrease of the spin-excitation energy Δ_Y at the ordering vector [30] which inevitably takes the role of the global minimum of the spectrum upon approaching the QCP, all in close accord with the data in Fig. 3. At the QCP, the asymptotic form of the spectrum adheres to the expected relativistic form. Above the QCP, the gap at the Y point reopens, with the spectrum experiencing a roughly uniform, Zeeman-like shift vs H . Remarkably, the high-field value of the gap at 9 T deep in the PM phase is also closely matched by the same model with no additional free parameters.

Summary. In summary, we have demonstrated that a combination of insights from the low-temperature specific heat data and theoretical modeling provide a comprehensive description of the ground state and excitations in a TL rare-earth anisotropic-exchange magnet, paving the way to a deeper understanding of a broad class of materials. The phenomenological constraints on the general microscopic model have resulted in precise identification of the CeCd_3As_3 magnetic ground state as a stripe phase with a remarkable level of certainty regarding the part of the phase diagram where it belongs.

This study is of immediate relevance to KCeS_2 [46], KErSe_2 [47], and isostructural CeCd_3P_3 [48], for which some of the same phenomenology has been observed. Future studies using thermodynamic and spectroscopic methods, such as low- T magnetization, nuclear and electronic magnetic resonance, and neutron and x-ray magnetic dichroism scattering, are expected to provide further insights into the nature of the crossover region in the H - T phase diagram and into the role of structural disorder in the static and dynamic properties of these materials. With more theoretical input, they should yield more systematic constraints on the model and elucidate the role of different terms in unusual magnetic states and excitations of anisotropic-exchange magnets.

Acknowledgments. Low-temperature specific heat, magnetization, and electrical resistivity measurements were supported by the U.S. Department of Energy, Office of Science, National Quantum Information Science Research Centers, Quantum Science Center (QSC). Sample synthesis and crystal structure determination were supported by the Los Alamos Laboratory Directed Research and Development Project No. 20190076ER. Scanning electron microscope and energy dispersive x-ray measurements were performed at the Center for Integrated Nanotechnologies, an Office of Science User Facility operated for the U.S. Department of Energy (DOE) Office of Science. Support from the Northwestern-Fermilab Center for Applied Physics and Superconducting Technologies and from the U.S. Department of Energy, Office of Science, Office of Workforce Development for Teachers and Scientists, Office of Science Graduate Student Research (SCGSR) program (K.E.A.) is acknowledged. The SCGSR program is administered by the Oak Ridge Institute for Science and Education for the DOE under Contract No. DE-SC0014664. The work

of A.L.C. was supported by the U.S. Department of Energy, Office of Science, Basic Energy Sciences under Awards No. DE-FG02-04ER46174 and No. DE-SC0021221. P.A.M. acknowledges support from JINR Grant for young scientists,

Grant No. 21-302-03. A.L.C. would like to thank the Kavli Institute for Theoretical Physics (KITP), where this work was advanced. KITP is supported by the National Science Foundation under Grant No. NSF PHY-1748958.

- [1] W. Witczak-Krempa, G. Chen, Y. B. Kim, and L. Balents, Correlated quantum phenomena in the strong spin-orbit regime, *Annu. Rev. Condens. Matter Phys.* **5**, 57 (2014).
- [2] L. Balents, Spin liquids in frustrated magnets, *Nature (London)* **464**, 199 (2010).
- [3] P. Anderson, Resonating valence bonds: A new kind of insulator, *Mater. Res. Bull.* **8**, 153 (1973).
- [4] Y. Li, P. Gegenwart, and A. A. Tsirlin, Spin liquids in geometrically perfect triangular antiferromagnets, *J. Phys.: Condens. Matter* **32**, 224004 (2020).
- [5] Y. Li, H. Liao, Z. Shang, S. Li, F. Jin, L. Ling, L. Zhang, Y. Zou, L. Pi, Z. Yang, J. Wang, Z. Wu, and Q. Zhang, Gapless quantum spin liquid ground state in the two-dimensional spin- $\frac{1}{2}$ triangular antiferromagnet YbMgGaO_4 , *Sci. Rep.* **5**, 16419 (2015).
- [6] M. B. Sanders, F. A. Cevallos, and R. J. Cava, Magnetism in the $\text{KBaRE}(\text{BO}_3)_2$ (RE=Sm, Eu, Gd, Tb, Dy, Ho, Er, Tm, Yb, Lu) series: Materials with a triangular rare earth lattice, *Mater. Res. Express* **4**, 036102 (2017).
- [7] M. Bordelon, E. Kenney, C. Liu, T. Hogan, L. Posthuma, M. Kavand, Y. Lu, M. Sherwin, N. P. Butch, C. Brown, M. J. Graf, L. Balents, and S. D. Wilson, Field-tunable quantum disordered ground state in the triangular-lattice antiferromagnet NaYbO_2 , *Nat. Phys.* **15**, 1058 (2019).
- [8] M. Baenitz, P. Schlender, J. Sichelschmidt, Y. A. Onykiienko, Z. Zangeneh, K. M. Ranjith, R. Sarkar, L. Hozoi, H. C. Walker, J. C. Orain, H. Yasuoka, J. van den Brink, H. H. Klauss, D. S. Inosov, and T. Doret, NaYbS_2 : A planar spin- $\frac{1}{2}$ triangular-lattice magnet and putative spin liquid, *Phys. Rev. B* **98**, 220409(R) (2018).
- [9] J. Sichelschmidt, B. Schmidt, P. Schlender, S. Khim, T. Doert, and M. Baenitz, Effective spin- $\frac{1}{2}$ moments on a Yb^{3+} triangular lattice: An ESR study, *JPS Conf. Proc.* **30**, 011096 (2020).
- [10] J. Sichelschmidt, P. Schlender, B. Schmidt, M. Baenitz, and T. Doert, Electron spin resonance on the spin- $\frac{1}{2}$ triangular magnet NaYbS_2 , *J. Phys.: Condens. Matter* **31**, 205601 (2019).
- [11] F. A. Cevallos, K. Stolze, T. Kong, and R. J. Cava, Anisotropic magnetic properties of the triangular plane lattice material TmMgGaO_4 , *Mater. Res. Bull.* **105**, 154 (2018).
- [12] Y. Li, S. Bachus, H. Deng, W. Schmidt, H. Thoma, V. Hutanu, Y. Tokiwa, A. A. Tsirlin, and P. Gegenwart, Partial Up-Up-Down Order with the Continuously Distributed Order Parameter in the Triangular Antiferromagnet TmMgGaO_4 , *Phys. Rev. X* **10**, 011007 (2020).
- [13] W. Liu, Z. Zhang, J. Ji, Y. Liu, J. Li, X. Wang, H. Lei, G. Chen, and Q. Zhang, Rare-earth chalcogenides: A large family of triangular lattice spin liquid candidates, *Chin. Phys. Lett.* **35**, 117501 (2018).
- [14] L. Ding, P. Manuel, S. Bachus, F. Grussler, P. Gegenwart, J. Singleton, R. D. Johnson, H. C. Walker, D. T. Adroja, A. D. Hillier, and A. A. Tsirlin, Gapless spin-liquid state in the structurally disorder-free triangular antiferromagnet NaYbO_2 , *Phys. Rev. B* **100**, 144432 (2019).
- [15] K. M. Ranjith, D. Dmytriieva, S. Khim, J. Sichelschmidt, S. Luther, D. Ehlers, H. Yasuoka, J. Wosnitza, A. A. Tsirlin, H. Kuhne, and M. Baenitz, Field-induced instability of the quantum spin liquid ground state in the $J_{\text{eff}} = \frac{1}{2}$ triangular-lattice compound NaYbO_2 , *Phys. Rev. B* **99**, 180401(R) (2019).
- [16] K. M. Ranjith, S. Luther, T. Reimann, B. Schmidt, P. Schlender, J. Sichelschmidt, H. Yasuoka, A. M. Strydom, Y. Skourski, J. Wosnitza, H. Kuhne, T. Doert, and M. Baenitz, Anisotropic field-induced ordering in the triangular-lattice quantum spin liquid NaYbSe_2 , *Phys. Rev. B* **100**, 224417 (2019).
- [17] J. Xing, L. D. Sanjeeva, J. Kim, G. R. Stewart, A. Podlesnyak, and A. S. Sefat, Field-induced magnetic transition and spin fluctuation in quantum spin liquid candidate CsYbSe_2 , *Phys. Rev. B* **100**, 220407(R) (2019).
- [18] J. Xing, L. D. Sanjeeva, J. Kim, W. R. Meier, A. F. May, Q. Zheng, R. Custelcean, G. R. Stewart, and A. S. Sefat, Synthesis, magnetization and heat capacity of triangular lattice materials NaErSe_2 and KErSe_2 , *Phys. Rev. Materials* **3**, 114413 (2019).
- [19] J. Xing, L. D. Sanjeeva, J. Kim, G. R. Stewart, M.-H. Du, F. A. Reboredo, R. Custelcean, and A. S. Sefat, Crystal synthesis and frustrated magnetism in triangular lattice CsRESe_2 (RE=La-Lu): Quantum spin-liquid candidates, *ACS Mater. Lett.* **2**, 71 (2020).
- [20] A. Scheie, V. O. Garlea, L. D. Sanjeeva, J. Xing, and A. S. Sefat, Crystal field hamiltonian and anisotropy in KErSe_2 and CsErSe_2 , *Phys. Rev. B* **101**, 144432 (2020).
- [21] J. Ma *et al.*, Spin-orbit-coupled triangular-lattice spin liquid in rare-earth chalcogenides, [arXiv:2002.09224](https://arxiv.org/abs/2002.09224).
- [22] N. Kabeya, T. Sakamoto, K. Hara, Y. Hara, S. Nakamura, K. Katoh, and A. Ochiai, Competing exchange interactions in lanthanide triangular lattice compounds LnZn_3P_3 (Ln=La-Nd, Sm, Gd), *J. Phys. Soc. Jpn.* **89**, 074707 (2020).
- [23] Y. D. Li, X. Wang, and G. Chen, Anisotropic spin model of strong spin-orbit-coupled triangular antiferromagnets, *Phys. Rev. B* **94**, 035107 (2016).
- [24] J. G. Rau and M. J. P. Gingras, Frustration and anisotropic exchange in ytterbium magnets with edge-shared octahedra, *Phys. Rev. B* **98**, 054408 (2018).
- [25] Z. Zhu, P. A. Maksimov, S. R. White, and A. L. Chernyshev, Disorder-Induced Mimicry of a Spin Liquid in YbMgGaO_4 , *Phys. Rev. Lett.* **119**, 157201 (2017).
- [26] Z. Zhu, P. A. Maksimov, S. R. White, and A. L. Chernyshev, Topography of Spin Liquids on a Triangular Lattice, *Phys. Rev. Lett.* **120**, 207203 (2018).
- [27] P. A. Maksimov, Z. Zhu, S. R. White, and A. L. Chernyshev, Anisotropic-Exchange Magnets on a Triangular Lattice: Spin Waves, Accidental Degeneracies, and Dual Spin Liquids, *Phys. Rev. X* **9**, 021017 (2019).
- [28] P. A. Maksimov and A. L. Chernyshev, Rethinking $\alpha\text{-RuCl}_3$, *Phys. Rev. Research* **2**, 033011 (2020).

- [29] S. R. Dunsiger, J. Lee, J. E. Sonier, and E. D. Mun, Long-range magnetic order in the anisotropic triangular lattice system CeCd_3As_3 , *Phys. Rev. B* **102**, 064405 (2020).
- [30] See Supplemental Material at <http://link.aps.org/supplemental/10.1103/PhysRevB.103.L180406> for technical details, additional magnetization, susceptibility and resistivity results, a phase diagram of model (3), consideration of different phases related to CeCd_3As_3 phenomenology, details of the spin-wave theory results for the spectrum in the AF stripe and PM phases and for Néel temperature, derivations of the asymptotic expressions for the specific heat in Eqs. (1) and (2), and model parameter considerations. It also includes Refs. [49–57].
- [31] J. Banda, B. K. Rai, H. Rosner, E. Morosan, C. Geibel, and M. Brando, Crystalline electric field of Ce in trigonal symmetry: CeIr_3Ge_7 as a model case, *Phys. Rev. B* **98**, 195120 (2018).
- [32] Y. Q. Liu, S. J. Zhang, J. L. Lv, S. K. Su, T. Dong, G. Chen, and N. L. Wang, Revealing a triangular lattice ising antiferromagnet in a single-crystal CeCd_3As_3 , [arXiv:1612.03720](https://arxiv.org/abs/1612.03720).
- [33] R. Ishii, S. Tanaka, K. Onuma, Y. Nambu, M. Tokunaga, T. Sakakibara, N. Kawashima, Y. Maeno, C. Broholm, and D. P. Gautreaux, Successive phase transitions and phase diagrams for the quasi-two-dimensional easy-axis triangular antiferromagnet $\text{Rb}_4\text{Mn}(\text{MoO}_4)_3$, *Europhys. Lett.* **94**, 17001 (2011).
- [34] M. Gvozdikova, P.-E. Melchy, and M.-E. Zhitomirsky, Magnetic phase diagrams of classical triangular and kagome antiferromagnets, *J. Phys.: Condens. Matter* **23**, 164209 (2011).
- [35] P. Sengupta, C. D. Batista, R. D. McDonald, S. Cox, J. Singleton, L. Huang, T. P. Papageorgiou, O. Ignatchik, T. Herrmannsdorfer, J. L. Manson, J. A. Schlueter, K. A. Funk, and J. Wosnitzer, Nonmonotonic field dependence of the néel temperature in the quasi-two-dimensional magnet $[\text{Cu}(\text{HF}_2)(\text{pyz})_2]\text{BF}_4$, *Phys. Rev. B* **79**, 060409(R) (2009).
- [36] B. Schmidt and P. Thalmeier, Frustrated two dimensional quantum magnets, *Phys. Rep.* **703**, 1 (2017).
- [37] V. Zapf, M. Jaime, and C. D. Batista, Bose-einstein condensation in quantum magnets, *Rev. Mod. Phys.* **86**, 563 (2014).
- [38] E. G. Batyev and L. S. Braginskii, Antiferromagnet in a strong magnetic field: Analogy with Bose gas, *Zh. Eksp. Teor. Fiz.* **87**, 1361 (1984) [*Sov. Phys. JETP* **60**(4), 781 (1984)].
- [39] O. A. Starykh, Unusual ordered phases of highly frustrated magnets: A review, *Rep. Prog. Phys.* **78**, 052502 (2015).
- [40] L. Seabra and N. Shannon, Competition between supersolid phases and magnetization plateaus in the frustrated easy-axis antiferromagnet on a triangular lattice, *Phys. Rev. B* **83**, 134412 (2011).
- [41] M. T. Hutchings, Point-charge calculations of energy levels of magnetic ions in crystalline electric fields, *Solid State Phys.* **16**, 227 (1964).
- [42] J. A. M. Paddison, M. Daum, Z. Dun, G. Ehlers, Y. Liu, M. B. Stone, H. Zhou, and M. Mourigal, Continuous excitations of the triangular-lattice quantum spin liquid YbMgGaO_4 , *Nat. Phys.* **13**, 117 (2017).
- [43] Y. Li, G. Chen, W. Tong, L. Pi, J. Liu, Z. Yang, X. Wang, and Q. Zhang, Rare-Earth Triangular Lattice Spin Liquid: A Single-Crystal Study of YbMgGaO_4 , *Phys. Rev. Lett.* **115**, 167203 (2015).
- [44] J. G. Rau, P. A. McClarty, and R. Moessner, Pseudo-Goldstone Gaps and Order-by-Quantum-Disorder in Frustrated Magnets, *Phys. Rev. Lett.* **121**, 237201 (2018).
- [45] S. Miyashita, Magnetic properties of ising-like heisenberg antiferromagnets on the triangular lattice, *J. Phys. Soc. Jpn.* **55**, 3605 (1986).
- [46] G. Bastien *et al.*, Long-range magnetic order in the $\tilde{S} = 1/2$ triangular lattice antiferromagnet KCeS_2 , *SciPost Phys.* **9**, 041 (2020).
- [47] J. Xing, K. M. Taddei, L. D. Sanjeewa, R. S. Fishman, M. Daum, M. Mourigal, C. dela Cruz, and A. S. Sefat, Stripe antiferromagnetic ground state of ideal triangular lattice KErSe_2 , *Phys. Rev. B* **103**, 144413 (2021).
- [48] J. Lee, A. Rabus, N. R. Lee-Hone, D. M. Broun, and E. Mun, The two-dimensional metallic triangular lattice antiferromagnet CeCd_3P_3 , *Phys. Rev. B* **99**, 245159 (2019).
- [49] E. Gopal, *Specific Heats at Low Temperatures*, International Cryogenics Monograph Series (Springer, New York, 1966).
- [50] Y. T. Fan, W. H. Lee, and Y. Y. Chen, Antiferromagnetic spin wave in Ce_2PdGe_6 , *Phys. Rev. B* **69**, 132401 (2004).
- [51] W. P. Halperin, F. Rasmussen, C. Archie, and R. Richardson, Properties of melting ^3He : Specific heat, entropy, latent heat, and temperature, *J. Low Temp. Phys.* **31**, 617 (1978).
- [52] P. Pagliuso, D. Garcia, E. Miranda, E. Granado, R. Serrano, C. Giles, J. Duque, R. Urbano, C. Rettori, J. Thompson, M. Hundley, and J. Sarro, Evolution of the magnetic properties and magnetic structures along the $\text{R}_m\text{MIn}_{3m+2}$ ($\text{R}=\text{Ce, Nd, Gd, Tb}$; $\text{M}=\text{Rh, Ir}$; and $m=1,2$) series of intermetallic compounds, *J. Appl. Phys.* **99**, 08P703 (2006).
- [53] S. S. Stoyko and A. Mar, Ternary rare-earth arsenides REZn_3As_3 ($\text{RE}=\text{La-Nd, Sm}$) and RECe_3As_3 ($\text{RE}=\text{La-Pr}$), *Inorg. Chem.* **50**, 11152 (2011).
- [54] Y. D. Li, Y. Shen, Y. Li, J. Zhao, and G. Chen, Effect of spin-orbit coupling on the effective-spin correlation in YbMgGaO_4 , *Phys. Rev. B* **97**, 125105 (2018).
- [55] E. V. Komleva, V. Y. Irkhin, I. V. Solovyev, M. I. Katsnelson, and S. V. Streltsov, Unconventional magnetism and electronic state in frustrated layered system PdCrO_2 , *Phys. Rev. B* **102**, 174438 (2020).
- [56] S. Higuchi, Y. Noshima, N. Shirakawa, M. Tsubota, and J. Kitagawa, Optical, transport and magnetic properties of new compound CeCd_3P_3 , *Mater. Res. Express* **3**, 056101 (2016).
- [57] W. M. Steinhardt, Z. Shi, A. Samarakoon, S. Dissanayake, D. Graf, Y. Liu, W. Zhu, C. Marjerrison, C. D. Batista, and S. Haravifard, Constraining the parameter space of a quantum spin liquid candidate in applied field with iterative optimization, [arXiv:1902.07825](https://arxiv.org/abs/1902.07825).